IOP Publishing Physics in Medicine and Biology

Phys. Med. Biol. **52** (2007) 5119–5130 doi:10.1088/0031-9155/52/17/001

Measurement of electric fields due to time-varying magnetic field gradients using dipole probes

P M Glover and R Bowtell

The Sir Peter Mansfield Magnetic Resonance Centre, School of Physics and Astronomy, University of Nottingham, Nottingham, NG7 2RD, UK

E-mail: Paul.Glover@Nottingham.ac.uk and Richard.Bowtell@Nottingham.ac.uk

Received 29 May 2007, in final form 5 July 2007
Published 7 August 2007
Online at stacks.iop.org/PMB/52/5119

Abstract

The operation of dipole probes in measuring electric fields in conductive media exposed to temporally varying magnetic fields is discussed. The potential measured by the probe can be thought of as originating from two contributions to the electric field, namely the gradient of the scalar electric potential and the temporal derivative of the magnetic vector potential. Using this analysis, it is shown that the exact form of the wire paths employed when using electric field probes to measure the effects of temporally varying magnetic fields is very important and this prediction is verified via simple experiments carried out using different probe geometries in a cylindrical sample exposed to a temporally varying, uniform magnetic field. Extending this work, a dipole probe has been used to measure the electric field induced in a cylindrical sample by gradient coils as used in magnetic resonance imaging (MRI). Analytic solutions for the electric field in an infinite cylinder are verified by comparison with experimental measurements. Deviations from the analytic solutions of the electric field for the x-gradient coil due to the finite length of the sample cylinder are also demonstrated.

(Some figures in this article are in colour only in the electronic version)

Introduction

In the field of MRI, it would be highly desirable to be able to measure directly the current density induced in the human body by the applied temporally varying magnetic fields (Schenck 2005, Schenck *et al* 1983). The measurement method would however necessarily be invasive and therefore has not been implemented. Despite this, action levels and limits for exposure of human subjects to time-varying magnetic fields have been defined in terms of a frequency-dependent current density within tissue (van Deventer *et al* 2005). What can be measured, of course, for exposure to temporally varying magnetic fields and all types of

movement in and around a scanner, is the rate of change of the magnetic field (Cavin *et al* 2006). The induced electric field and current density must then be inferred via numerical modelling (Bencsik *et al* 2007, Crozier and Liu 2005, Liu *et al* 2003a, 2003b, Nadeem *et al* 2003, Wang and Eisenberg 1994). Electric fields have however been measured routinely in phantoms, *in vitro* and *in vivo* for many years over a range of frequencies (Deutsch 1968, Jarzembski *et al* 1970, Kaune and Forsythe 1985, Lang *et al* 1969, McLeod *et al* 1983, Miller 1991, Tay *et al* 1989, Yunokuchi and Cohen 1991). Interest in radio frequency and power line effects has driven the development of specific methods for both high (10–100 MHz) (Taylor *et al* 1997) and low (50–5000 Hz) (Miller 1991) frequency measurements. At radio frequency (RF), the coupling of the probe to the electric field is different to that occurring at low frequency and the RF measurement is not considered further here, although similar arguments can be followed.

Techniques for measuring induced electric fields and current density fall into two separate categories. First there are the loaded probe methods which measure current directly (Deutsch 1968, Jarzembski *et al* 1970, Lang *et al* 1969, Swiontek *et al* 1976, Tay *et al* 1989). In this approach, the probe replaces a volume of tissue with an equivalent conductive path routed through a current amplifier. Advantages of this method are as follows: the direct measurement of current density; immunity to induced electric fields in the leads; the need for just two contacts (i.e. no extra reference contact is required); and accuracy of measurement in low conductivity media. Disadvantages include the relatively large displacement of tissue volume by the probe; the requirement that the current amplifier input impedance be adjustable; and the need for very low contact impedance, which is difficult to fulfil at low frequency. These disadvantages make such probes difficult to employ for general purpose measurements and they are not considered further here.

Second, there are electric field measurement methods based on the use of probes formed from small dipole elements (Hart and Wood 1991, Kaune and Forsythe 1985, Miller 1991, Yunokuchi and Cohen 1991). Such probes have the advantages of producing a lower displaced tissue volume, being simpler to construct and having fewer constraints regarding contact resistance. The latter advantage is particularly relevant to measuring very low frequency induced currents. With this approach, although the electric field can be measured accurately, the current density can only be inferred by knowing or measuring the magnitude of the local electrical conductivity. Disadvantages of the dipole method are low immunity to electromagnetic interference and poor low frequency stability. There is also a requirement for a reference electrode to be present. This reference, which is needed to provide a bias current to the high impedance amplifier and to establish a fixed potential point for correct amplifier operation, can be built into the probe or applied separately. The measured electric field is taken as the difference in potential measured between the tips of the probe divided by the distance between the tips. The current density is then obtained by multiplying the electric field by the measured or assumed conductivity of the tissue or fluid.

It is also possible to use a complete loop to detect the changing magnetic field. This type of measurement can only be used to infer the electric field external to any conductive samples and cannot be used to measure the electric field within a sample (Epstein *et al* 1990, Salinas *et al* 2007). Such techniques are not considered further here. Branston and Tofts (1991) provide a further discussion of techniques used for electric field measurements.

It has previously been shown that dipole probes work correctly when the current in the tissue is supplied by a potential difference i.e. via an externally applied electric field (Kaune and Forsythe 1985). However, when current is induced by a temporally varying magnetic field, the difference in potential at the two tips does not necessarily provide a measurement of the total electric field. This vital point appears to have been missed in the literature, or at least

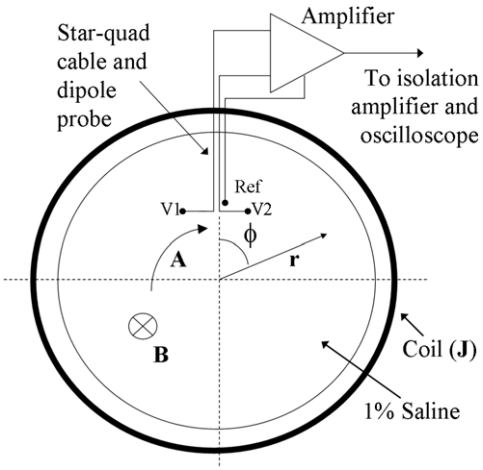

Figure 1. Coil and probe geometry showing the amplifier, dipole probe and measurement amplifier.

not expressly stated (Branston and Tofts 1991, Hart and Wood 1991, Miller 1991, Yunokuchi and Cohen 1991). Despite this fact, the potential measured by an amplifier connected to the probe yields the correct value of the electric field when the probe is formed from a short, dipole element such that the wires which connect the probe tips to the amplifier form a short straight line running directly between the tips.

This paper aims to correct some misconceptions that have been promulgated in the literature on the measurement of magnetically induced electric fields and to show how measurements can be correctly related to the magnetic field via analysis of the vector, magnetic and scalar, electric potentials (Bencsik *et al* 2003, Jackson 1998). Experiments involving two different probe designs applied to cylindrical samples exposed to a temporally varying, but spatially uniform magnetic field provide some insight into the different contributions to the measured voltage. In addition a small dipole probe has been constructed and used to measure the electric field induced in a uniform cylindrical conducting phantom by temporally varying magnetic field gradients. The results are shown to be in good agreement with the predictions of previously described analytic expressions (Bencsik *et al* 2003, Bowtell and Bowley 2000).

Theory

Faraday's law states that the electromotive force (EMF) generated around a complete circuit is equal to the negative of the rate of change of total magnetic flux linked by the circuit. The EMF is also given by the closed loop integral of the electric field around the circuit. A dipole probe constructed from two insulated wires, each tipped with an electrode (see figure 1 and Hart and Wood (1991)), does not apparently form a complete loop and the incomplete circuit therefore does not define an area over which to calculate the changing magnetic flux. We show below that use of the magnetic, vector potential overcomes this apparent problem and provides a full explanation of the dipole probe operation.

The magnetic flux density $\mathbf{B}$ is related to the vector potential, $\mathbf{A}$, via the relation $\mathbf{B} = \nabla \times \mathbf{A}$ and inserting this expression into the differential form of Faraday's equation, shows that the electric field induced by a changing magnetic field can be written as

$$\mathbf{E} = -\nabla V - \partial \mathbf{A}/\partial t \tag{1}$$

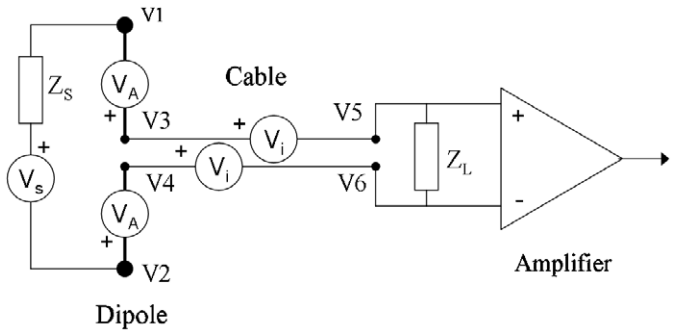

Figure 2. The dipole probe showing direct and induced potentials.

where V is the scalar, electric potential (Jackson 1998). Although the vector potential completely defines the magnetic field, the reverse is not true and it is always possible to add the grad of a scalar to $\mathbf{A}$ without changing the magnetic field. We can fix the vector potential by adopting a particular gauge and in particular when using the Coulomb gauge, the vector potential $\mathbf{A}$ can be calculated from a volume integral of the current density, $\mathbf{J}$. In the quasi-static situation considered here, this relation is

$$\mathbf{A}(\mathbf{r}) = \frac{\mu_0}{4\pi} \int \frac{\mathbf{J}(\mathbf{r}')}{|\mathbf{r} - \mathbf{r}'|} \, \mathrm{d}\tau \tag{2}$$

where $\mathbf{r}$ and $\mathbf{r}'$ are vectors defining the positions of the field point and the current density, respectively (Jackson 1998). The scalar potential term, V, in equation (1) is then found by applying boundary conditions at the interfaces between regions of different electrical conductivities. The appropriate boundary conditions relate to continuity of the normal component of the current density, $\mathbf{J}$, and the tangential component of the electric field.

A high-impedance voltage amplifier connected to a probe is only sensitive to the difference in electric potential at its inputs. From the previous discussion, it is clear that a measurement of the total electric field must be sensitive to both terms on the right-hand side of equation (1) which shows that the scalar potential difference at the probe tips does not fully characterize the electric field. However, what the amplifier actually measures is the difference between the potentials at the tips of the dipole probe plus an additional scalar potential difference that is induced in the wire leads which connect the electrode tips to the amplifier as depicted in figure 2. The scalar potential, V, present within the sample determines the potential difference across the tips ($V_1 - V_2$) and is shown as a source of potential, V_S, in this figure. The resistance of the sample and the electrode impedance are lumped together as source impedance, Z_S. Assuming that the impedance of the amplifier, Z_L, is high, no current can flow in the wires of the dipole probe, which means that a potential difference $\partial\mathbf{A}/\partial t \cdot \mathbf{dl}$ must be produced across each element, $\mathbf{dl}$, of the probe wires in order to cancel the effect of the temporally varying vector potential, otherwise current would flow. For the dipole element shown in figure 2, an additional potential ($2V_A$) is therefore developed due to the line integral of $\partial\mathbf{A}/\partial t$ along the path of the wires between the probe tips, such that potential difference generated by the dipole probe is given by $V_3 - V_4 = V_1 - V_2 + 2V_A$.

The potential difference at the input to the amplifier, $V_5 - V_6$, also depends on the integral of $\partial\mathbf{A}/\partial t$ along the leads connecting the dipole probe to the amplifier. However, if these leads are made suitably coincident then the induced voltage, V_i, in each lead will be equal and

opposite, so that $V_3 - V_4 = V_5 - V_6$, and the amplifier senses only the potential difference produced by the dipole probe. Assuming that the tips of the dipole probe are close together such that the vector and scalar potentials do not vary significantly over the vector, **l**, joining the probe tips, then we can write

$$V_3 - V_4 = V_1 - V_2 + 2V_A \approx (\nabla V + \partial \mathbf{A}/\partial t) \cdot \mathbf{dl} = -\mathbf{E} \cdot \mathbf{dl} \tag{3}$$

which indicates that the voltage measured by the dipole probe depends on the component of the electric field along the dipole. It can also be inferred from the above analysis that when the connections of the probe tips to the amplifier deviate from the dipole form, the voltage measured by the amplifier is no longer a measure of the electric field near the probe tips. This is a consequence of the non-conservative nature of $\partial \mathbf{A}/\partial t$ which means that the voltage developed by this term depends on the path of integration. When constructing dipole probes, the tip separation must be made small compared with the length scale over which the induced electric field varies significantly if the probe is to produce a correct measurement of the local electric field. Measurement of the voltage produced in three, separate, orthogonal dipoles would be required to characterize the electric field fully.

When using dipole probes, the nature of the contact at the electrode tips can vary considerably without significantly changing the measurement accuracy (Mirtaheri *et al* 2005). The contact impedance variation (due to the contact-electrolyte double-layer capacitance) is only significant for low-frequency measurements. Variations in contact potential are therefore more significant at lower frequency, but can be disregarded for frequencies above a few Hz. The probe response will also roll-off above the cut-off frequency caused by the equivalent source impedance and the capacitance of the cable. At the range of frequencies encountered in MRI gradient switching neither of these effects are likely to be a problem.

If a dipole probe is used in very low conductivity samples or air then the source impedance, Z_S, becomes large and the potential V_S is dominated by electrostatic effects. Hence the above assumptions are no longer true and the dipole probe will not measure the magnetically induced electric field correctly.

We now analyse the form of the induced electric field for the case of a cylindrical, weakly conducting phantom exposed to a temporally varying uniform field due to a solenoidal coil. The analysis provides some insight into the form of the voltages measured using the two different probe types in the experiments described later. For the simple short solenoid used in our experiments (see figure 1), the vector potential is assumed to be close in form to that produced by an infinite solenoid, which can be written as $\mathbf{A} = -1/2\ \mathbf{r} \times \mathbf{B}$ where **r** is the position vector measured relative to the centre of the coil. In cylindrical polar coordinates with the magnetic field directed along the z-axis, only the azimuthal component of the vector potential is nonzero and can be written as $A_\phi = \frac{1}{2} r B_z$. In any particular conductive sample, the scalar potential term can be derived from consideration of the boundary conditions. For the simple case of a uniform sample of finite electrical conductivity surrounded by a region of zero conductivity, continuity of current flow requires that the normal component of **E** is zero at the boundary of the sample. In the geometry shown in figure 1 the normal component of **A** is zero over the whole boundary. Hence, when a cylinder of uniform conductivity is positioned coaxially with the coil of a solenoidal electromagnet which generates a uniform magnetic field that is changing in time, the term ∇V is zero throughout the conducting cylinder. A calculation of the electric field purely from a measurement of the potential difference at the tips of a dipole probe would clearly therefore yield an incorrect result. Using equation (1) which takes into account the effect of the temporally varying vector potential we find that the electric field is actually given by $E_\phi = -\partial A_\phi/\partial t = -\frac{1}{2} r \partial B_z/\partial t$ as expected.

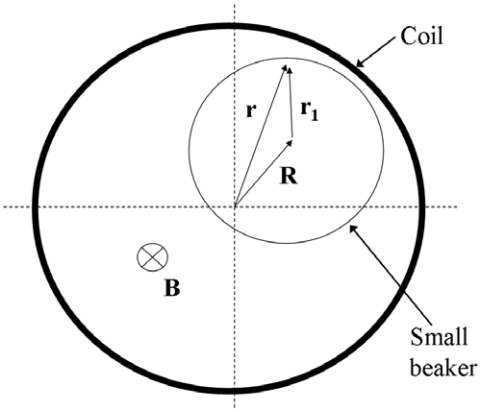

Figure 3. Geometry for an offset beaker.

We now consider the case where the cylindrical phantom is moved off axis as shown in figure 3. In considering this situation, it is important to remember that the vector potential is unaffected by the presence of low conductivity samples such as tissue and equivalent phantoms since the vector potential is defined solely by the coil current and geometry (equation (2)). Consequently the probe experiences the same vector potential when it is placed in the same position relative to the coil independent of the sample geometry. In particular this means that wires that are arranged radially with respect to the solenoidal coil are always orthogonal to the vector potential and so do not experience induced voltages due to the line integral of $\partial\mathbf{A}/\partial t$. For the geometry shown in figure 3, in which the vector $\mathbf{R}$ joins the phantom and coil axes, it is simple to show that the scalar potential must take the form $V(\mathbf{r}_1) = \frac{1}{2}\mathbf{r}_1 \cdot (\partial\mathbf{B}/\partial t \times \mathbf{R})$ within the phantom to ensure that the normal component of the electric field at the boundary is zero. Using equation (1), the electric field is then given by

$$\mathbf{E} = -\nabla\left(\frac{1}{2}\mathbf{r}_1 \cdot (\partial\mathbf{B}/\partial t \times \mathbf{R})\right) - \frac{\partial}{\partial t}\left(\frac{1}{2}(\mathbf{B} \times (\mathbf{r}_1 + \mathbf{R})\right) = -\frac{1}{2}\mathbf{r}_1 \times \partial\mathbf{B}/\partial t \tag{4}$$

which viewed in the cylindrical polar coordinate systems defined by the sample cylinder is identical in form to the field produced when the sample is centred within the coil. This is clearly as expected since for a long solenoid, the magnetic field experienced by the cylindrical phantom is independent of the radial offset.

Methods

Two simple separate dipole element probes both with a 50 mm tip separation were constructed from insulated copper wire as shown in figure 4. One probe had 50 mm radial elements coming together at a central point, which we define as the origin, and making an angle of 57° to one another and the other had arc elements arranged on a 50 mm radius. The radial wires of the arc probe were twisted together and travelled from the origin to the circumference position midway between the two tips. A reference electrode (Miller 1991) was positioned near the origin within the saline for all measurements. When making comparable measurements with the two probes, the tips were identically positioned within the saline and were 50 mm apart. The ends of the bare copper wires were coated with silver conductive paint (RS Components UK stock 186-3593) which was then baked to form a robust conductive silver layer. 'Chloriding'

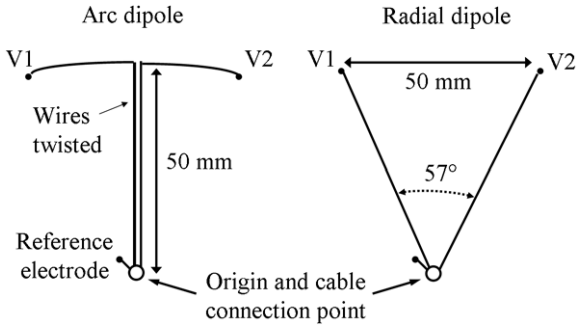

Figure 4. Arc and radial probe construction.

of the electrodes may also be carried out if required and is recommended for low frequency measurements (Geddes *et al* 1969) although this procedure was not used for the measurements described here. Star-quad balanced cable (Van Damme type 278-801-000) was used to form the leads running from the origin point of each probe to a high impedance amplifier. The use of a star-quad cable (where four cores are used as two pairs with diametrically opposite cores connected) ensured a greater immunity to electromagnetic interference. In this type of cable, the wire arrangement means that induced voltages resulting from electromagnetic interference are cancelled for any elemental cable length rather than relying on cancellation along the twist distance of a normal twisted pair. Use of this type of cable is essential if the cable has to pass through regions of high switched magnetic field as may be the case in a gradient coil. The amplifier has a gain of 100 and is based on an INA114 (Texas Instruments, USA) instrumentation amplifier device (figure 1). This amplifier was fully electrically isolated via an ISO124 amplifier (Texas Instruments, USA) and RP1212D power supply (RECOM International Power GmbH, Austria) in order that simultaneous multiple point measurements could be made using other channels if required in the future.

A solenoidal coil composed of 50 turns was wound on a former of 145 mm diameter and 50 mm length yielding an efficiency of 490 μT A^{-1} at the coil centre. A sinusoidal current of 0.39 A peak amplitude and 500 Hz frequency was passed through the solenoid using a signal generator and small power amplifier giving a peak field and rate of change of field with time of 190 μT and 0.6 T s^{-1}, respectively. Two glass dishes of 110 and 65 mm diameter, filled with approximately 1% saline to a depth of 50 mm were placed in the coil in the central and offset positions shown in figures 1 and 3. The saline conductivity was not measured as only electric field measurements are reported here. The smaller dish was placed such that the central axis of the solenoid fell within the fluid. Both probes could be placed in either dish in essentially the same position relative to the coil.

A third probe of more conventional design was constructed based on short, straight dipole elements (Hart and Wood 1991) with a 20 mm tip separation and inclusion of an additional central reference tip (Miller 1991). The probe was calibrated by using a known electric field in a long trough of saline with a square cross-section. This probe was then used for measurements of electric field in a MRI gradient coil system. The gradient coil used has been described elsewhere (Bowtell and Peters 1999) and the method for calculating the electric fields and potentials has also been demonstrated (Bowtell and Bowley 2000). The gradient coil set was not positioned in the scanner for these measurements, but placed on the floor with its z-axis vertical. A 258 mm diameter 900 mm length cylinder filled with 0.5% saline was placed co-axially with the gradient set. The gradient was driven from the scanner system

with a pulsed (ten cycles of) sinusoidal waveform of 500 Hz frequency. A peak current of 43.8 A was used, giving peak gradient values of 4.21 mT m^{-1} and 16.6 mT m^{-1} for the x- and z-gradient coils, respectively. At 500 Hz, the peak rate of change of magnetic field gradient is therefore 13.2 T m^{-1} s^{-1} and 52.0 T m^{-1} s^{-1} for the x- and z-gradients, respectively. The induced voltage was read directly from an oscilloscope set to average eight cycles and eight repetitions and to display the RMS voltage. The probe cable was inserted through a long 6 mm diameter Perspex tube which was used to position the probe at the desired location. A simple arrangement based on a clamp screw was employed to allow the probe to be located at any desired z-axis position. Graduations marked on the cylinder and support bar allowed for any x–y location to be selected. Accuracy of positioning in each axis was ± 1 mm. Measurements of E_x and E_y were made on a 20 mm grid for a complete transverse (x–y) plane using both the z-gradient ($z = 50$ mm) and the x-gradient ($z = 0$ mm). In addition the azimuthal component of the electric field (E_ϕ) was measured at a radius of 100 mm for a range of z positions. For the x-gradient the azimuthal angle used was 40° corresponding to the maximum value of E_ϕ at that radius. Due to the presence of cable connections to the gradient coil the measurement x and y axes were offset from the gradient x and y axes used by 40°. The measurement of the axial dependence of electric field was repeated for the x-gradient, but with approximately 100 mm of saline removed from the cylinder to give a shorter and axially asymmetric conductive medium. The calibrated electric field measurements have an accuracy of $\pm 2\%$.

Results

In the larger 110 mm diameter dish, the arc probe gave a voltage of 780 ± 20 μV peak which corresponds to a peak electric field of 15.5 ± 0.4 mV m^{-1}. Since the electric field is sampled at a radius of 50 mm, and the magnetic field varies at 500 Hz this measurement yields an estimate of the peak uniform magnetic field generated by the solenoid of 194 ± 6 μT, which is in good agreement with the value calculated from the applied current and coil efficiency. Using the radial probe in the same dish, a null was found in the measured voltage when the probe and cylinder centres coincided to an estimated positional accuracy of ± 2 mm. When the large cylindrical dish was replaced with the smaller one and the absolute positions of the probes (relative to the coil) retained, the peak measurements became 310 ± 15 μV and 530 ± 20 μV peak for the radial and arc probes, respectively. No null could be found using the radial probe wherever the small dish was placed in the coil.

Measurements of the electric field in the cylindrical container placed in the gradient coil show excellent agreement with the expected analytic results. Figures 5(a) and (b) demonstrate the form of the electric field produced in a transverse plane by temporally varying z- and x-gradients, respectively. For the z-gradient, only the azimuthal component of the electric field is nonzero and its amplitude is proportional to the radial position. For the x-gradient the electric field is mainly directed normal to the gradient direction and is symmetric with respect to the x- and y-axes defined by the coil. The net current flow across the transverse plane is balanced by the z-component of the current density and there is also a reversal of the sign of dominant in-plane current flow in planes that are axially displaced from the coil centre in the positive and negative directions. The latter can be seen in figure 6(b) in which the azimuthal electric field at a radius of 100 mm is plotted as a function of the z position. A similar plot for the z-gradient is shown in figure 6(a). Calculated values of the electric field in an infinite cylinder are also shown superimposed on the plots of the experimental data in figure 6.

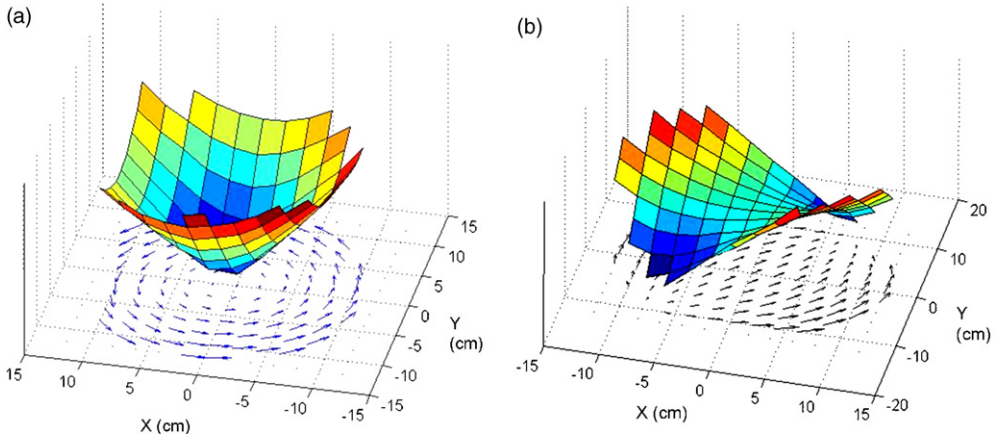

Figure 5. The induced electric fields measured within a saline filled cylinder in the transverse (x–y) plane of the gradient coils. The plots are in arbitrary units and show the modulus of the electric field as a surface plot and the vector of the electric field as an arrow plot. (a) Data recorded from the $z = 0.05$ m plane while the z-gradient coil was driven. (b) Data recorded from the $z = 0.0$ m plane while the x-gradient coil was driven.

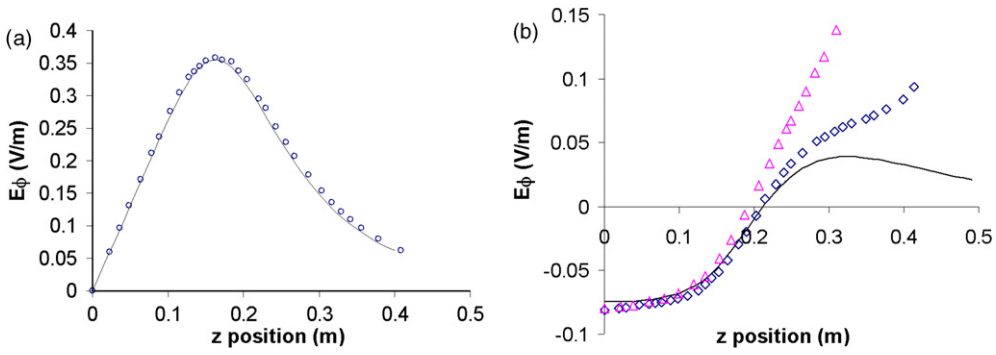

Figure 6. (a) The azimuthal component of the electric field induced by the z gradient coil as a function of the axial position and measured at a radius of 0.10 m. (b) The azimuthal component of the electric field induced by the x gradient coil as a function of the axial position and measured at a radius of 0.10 m and an azimuthal angle of 40°. Circles indicate measurements from a 0.83 m length cylinder of saline (meniscus at $z \sim 0.42$ m) and triangles show results produced when the liquid level was reduced by 0.1 m. For both graphs the solid lines show the analytically calculated values of electric field for an infinite cylinder.

Discussion

The measurements made using the radial and arc probes with identical electrode spacings show that the paths taken by the leads which connect the electrodes to the amplifier have a very strong influence on the measured voltage. In particular when the radial probe was centred within the cylindrical phantom and co-axial solenoid, zero voltage was measured, although the arc probe with identically positioned electrode tips gave a measurement of 780 μV. Dividing the latter measurement by the electrode separation yields a value of the induced electric field, which agrees well with the expected value. Using the analysis outlined

in the theory section, the null measurement from the radial probe can be explained as resulting from the orthogonality of the radial wires and the vector potential, which means that no potential difference is induced in the wires, along with the spatial invariance of the scalar potential, which means that the potential difference between the electrode tips is zero. In this picture, the full voltage measured by the arc probe can be attributed to the integral of $\partial\mathbf{A}/\partial t$ along the arc of wire linking the probe tips.

When the phantom is displaced within the solenoid, but the probes are kept in the same position relative to the coil, the voltages measured by both probes are changed. This shows that the probes are not just sensitive to the rate of change of vector potential occurring along the lead paths, which is unchanged by displacement of the sample. Changes in the measured voltage can be explained as resulting from the presence of a spatially varying scalar potential in the offset phantom, which causes a 310 μV potential difference between the electrode tips. Subtracting this potential difference from the 780 μV, previously shown to be induced along the wires of the arc probe by the vector potential, approximately yields the 530 μV voltage measured using the arc probe in the offset cylindrical sample. This voltage provides a rough estimate of the peak electric field in the offset phantom of 10.6 mV m^{-1}, although the fact that the electrode separation is similar in size to the phantom diameter, while the probe wires do not follow an azimuthal path, limits the accuracy of this measurement. The inability to find a voltage null with the radial probe in the smaller dish results from the fact that the radial arms of the probe are too long to allow the probe to be positioned with its origin at the dish centre. If a smaller radial probe is used in the smaller dish then a null would be found with the probe origin at (or near in practice) the centre of the dish wherever the dish is placed in the solenoid coil.

In the experiments carried out on the gradient coil set, the measured electric field closely matches the analytic predictions for both x- and z-gradients. Small discrepancies may result from errors in positioning and aligning a water-filled cylinder and gradient set of 50 and 200 kg respective weight and from limited accuracy of positioning of the probe (about $\pm 5\%$). However, the main deviation from the analytic expression occurred at points near to the upper end of the cylinder for x-gradient switching. This deviation results from the air–water boundary at the top of the cylindrical phantom, at which the normal component of the electric field must be zero. The spatially varying scalar potential needed to cancel the axial component of the rate of change of vector potential at this boundary causes a significant deviation of the electric field from that predicted by the infinite cylinder expressions (Bencsik *et al* 2003, Bowtell and Bowley 2000) in regions close to the meniscus. Reducing the length of the water cylinder caused a larger deviation of measured and calculated fields. This behaviour is not seen when using the z-gradient as there are no z-components of vector potential or electric field with this geometry.

Conclusions

The experiments described here provide new information which helps to clarify the mode of operation of electric field probes in measurements carried out in the quasi-static regime. Improved understanding in this area, based on an interpretation of the vector and scalar potentials, should assist in the future design of electric field probes for induced current measurements. In addition, this work highlights the danger of using only one of the vector magnetic or scalar electric potentials to define the electric field when temporally varying magnetic fields are present. Measurements of the electric field induced in a conductive cylinder by magnetic field gradients of the form used in MRI are shown for the first time to be in good agreement with analytic solutions.

Acknowledgments

We thank the UK Medical Research and Engineering and Physical Sciences Research Councils for their support of this project (grant number G9900259). We thank Ian Thexton and Jeffrey Smith for technical support.

References

Bencsik M, Bowtell R and Bowley R M 2003 Using the vector potential in evaluating the likelihood of peripheral nerve stimulation due to switched magnetic field gradients *Magn. Reson. Med.* **50** 405–10

Bencsik M, Bowtell R and Bowley R M 2007 Electric fields in the human body by time-varying magnetic field gradients: numerical calculations and correlation analysis *Phys. Med. Biol.* **52** 1–17

Bowtell R and Bowley R M 2000 Analytic calculations of the e-fields induced by time-varying magnetic fields generated by cylindrical gradient coils *Magn. Reson. Med.* **44** 782–90

Bowtell R and Peters A 1999 Analytic approach to the design of transverse gradient coils with co-axial return paths *Magn. Reson. Med.* **41** 600–8

Branston N M and Tofts P S 1991 Analysis of the distribution of currents induced by a changing magnetic-field in a volume conductor *Phys. Med. Biol.* **36** 161–8

Cavin I D, Glover P M, Bowtell R W and Gowland P A 2006 Thresholds for perceiving a metallic taste at large magnetic field *14th Ann. Meeting of the Int. Society for Magnetic Resonance in Medicine (Seattle, WA, USA)*

Crozier S and Liu F 2005 Numerical evaluation of the fields induced by body motion in or near high-field MRI scanners *Prog. Biophys. Mol. Biol.* **87** 267–78

Deutsch S 1968 A probe to monitor electroanesthesia current density *IEEE Trans. Biomed. Eng.* **15** 130–1

Epstein C M, Schwartzberg D G, Davey K R and Sudderth D B 1990 Localizing the site of magnetic brain-stimulation in humans *Neurology* **40** 666–70

Geddes L A, Baker L E and Moore A G 1969 Optimum electrolytic chloriding of silver electrodes *Med. Biol. Eng.* **7** 49–56

Hart F X and Wood K W 1991 Eddy-current distributions—their calculation with a spreadsheet and their measurement with a dual dipole antenna probe *Am. J. Phys.* **59** 461–7

Jackson J D 1998 *Classical Electrodynamics* (New York: Wiley)

Jarzembski W B, Larson S J and Sances A 1970 Evaluation of specific cerebral impedance and cerebral current density *Ann. NY Acad. Sci.* **170** 476–90

Kaune W T and Forsythe W C 1985 Current densities measured in human models exposed to 60-Hz electric-fields *Bioelectromagnetics* **6** 13–32

Lang J, Sances A and Larson S J 1969 Determination of specific cerebral impedance and cerebral current density during application of diffuse electrical currents *Med. Biol. Eng.* **7** 517–25

Liu F, Xia L and Crozier S 2003a Influence of magnetically-induced e-fields on cardiac electric activity during MRI: a modeling study *Magn. Reson. Med.* **50** 1180–8

Liu F, Zhao H W and Crozier S 2003b Calculation of electric fields induced by body and head motion in high-field MRI *J. Magn. Reson.* **161** 99–107

McLeod B R, Pilla A A and Sampsel M W 1983 Electromagnetic-fields induced by Helmholtz aiding coils inside saline-filled boundaries *Bioelectromagnetics* **4** 357–70

Miller D L 1991 Miniature-probe measurements of electric-fields and currents induced by a 60-Hz magnetic-field in rat and human models *Bioelectromagnetics* **12** 157–71

Mirtaheri P, Grimnes S and Martinsen O G 2005 Electrode polarization impedance in weak NaCl aqueous solutions *IEEE Trans. Biomed. Eng.* **52** 2093–9

Nadeem M, Thorlin T, Gandhi O P and Persson M 2003 Computation of electric and magnetic stimulation in human head using the 3D impedance method *IEEE Trans. Biomed. Eng.* **50** 900–7

Salinas F S, Lancaster J L and Fox P T 2007 Detailed 3D models of the induced electric field of transcranial magnetic stimulation coils *Phys. Med. Biol.* **52** 2879–92

Schenck J F 2005 Physical interactions of static magnetic fields with living tissues *Prog. Biophys. Mol. Biol.* **87** 185–204

Schenck J F, Edelstein W A, Hart H R, Williams C S, Bean C P, Bottomley P A and Redington R W 1983 Switched gradients and rapidly changing magnetic-field hazards in NMR imaging *Med. Phys.* **10** 133

Swiontek T J, Sances A, Larson S J, Ackmann J J, Cusick J F, Meyer G A and Millar E A 1976 Spinal-cord implant studies *IEEE Trans. Biomed. Eng.* **23** 307–12

Tay G, Chilbert M, Battocletti J, Sances A, Swiontek T and Kurakami C 1989 Measurement of magnetically induced current-density in saline and *in-vivo Proc. of the 11th Ann. Int. Conf. of the IEEE Engineering in Medicine and Biology Society* pp 1167–8

Taylor H C, Burl M and Hand J W 1997 Design and calibration of electric field probes in the range 10–120 MHz *Phys. Med. Biol.* **42** 1387–94

van Deventer T E, Saunders R and Repacholi M H 2005 WHO health risk assessment process for static fields *Prog. Biophys. Mol. Biol.* **87** 355–3

Wang W P and Eisenberg S R 1994 A 3-dimensional finite-element method for computing magnetically induced currents in tissues *IEEE Trans. Magn.* **30** 5015–23

Yunokuchi K and Cohen D 1991 Developing a more focal magnetic stimulator: 2. Fabricating coils and measuring induced current distributions *J. Clin. Neurophysiol.* **8** 112–20